Intrinsic Magnetic Properties of Ce₂Fe₁₄B Modified by Al, Ni, or Si

Kayode Orimoloye [1], Dominic H. Ryan [2], Frederick E. Pinkerton [3] and Mamoun Medraj [1,*]

[1] Department of Mechanical, Industrial and Aerospace Engineering, Concordia University, Montreal, QC H3G 1M8, Canada; orimoloyekayode@yahoo.com
[2] Physics Department and Centre for the Physics of Materials, McGill University, Montreal, QC H3A 2T8, Canada; dominic@physics.mcgill.ca
[3] Chemical and Materials Systems Lab, General Motors R&D Center, 30500 Mound Rd., Warren, MI 48090, USA; fpinkerton81@gmail.com
[*] Correspondence: mmedraj@encs.concordia.ca; Tel.: +1-514-848-2424 (ext. 3146)

Featured Application: This is a contribution towards developing low-cost Fe-based permanent magnets that are suitable for the automobile industry.

Abstract: Intrinsic magnetic properties (saturation magnetization, anisotropy fields, and Curie temperatures) of $Ce_2Fe_{14}B$ doped with Al, Ni, and Si are presented. Substitution for Fe by these elements leads to the formation of solid solutions that crystallize in the tetragonal $Nd_2Fe_{14}B$ structure. Substituting Al, Ni, or Si for Fe leads to a decrease in both the saturation magnetization and the anisotropy field of $Ce_2Fe_{14}B$. Ni and Si increase the Curie temperature of $Ce_2Fe_{14}B$ while Al reduces it. While, for the $Ce_2(Fe_{14-x}T_x)B$ containing Ni, a maximum Curie temperature of 210 °C was observed at 9 atom % Ni ($x = 1.45$), the highest value of 252 °C was found for the $Ce_2Fe_{14}B$ containing 14 atom % Si ($x = 2.26$).

1. Introduction

The demand for Nd–Fe–B permanent magnets continues to increase due to their superior magnetic properties, despite the relatively high price of Nd and its restricted supply [1–7]. The low cost and availability of Ce have driven interest in developing Ce-based permanent magnets to replace expensive $Nd_2Fe_{14}B$ magnets in certain applications [7–19]. This has resulted in investigation of $Ce_2Fe_{14}B$ and its alloys [20–26]. $Ce_2Fe_{14}B$ has intrinsic magnetic properties [3–7] that are inferior to those observed for the $Nd_2Fe_{14}B$ [4,6,7], but they can be improved using a fourth element to replace some of the Fe in $Ce_2Fe_{14}B$. Studies of $Nd_2(Fe_{14-x}T_x)B$, where T = Al, Ni, and Si have shown that Ni and Si increase the Curie temperature (T_C) and Al significantly increases coercivity [27–31]. Homogeneity ranges for $Ce_2(Fe_{14-x}Ni_x)B$, $Ce_2(Fe_{14-x}Si_x)B$, and $Ce_2(Fe_{14-x}Al_x)B$ solid solutions have been found to be ($0 \leq x_{Ni} \leq 1.5$), ($0 \leq x_{Si} \leq 2.33$), and ($0 \leq x_{Al} \leq 2.5$), respectively, at 900 °C, and the details of the phase equilibria in these systems are reported elsewhere [32]. The dopant concentrations used throughout this paper are the actual values substituting for Fe in the $Ce_2Fe_{14}B$ phase as determined by scanning electron microscopy (SEM) combined with wavelength-dispersive X-ray spectroscopy (WDS). $Ce_2(Fe_{14-x}T_x)B$ solid solutions, where T = Al, Ni, and Si, show visible magnetic domains using magnetic force microscopy (MFM) analysis, and more details can be found in [32]. The aim of this work is to quantify the changes in the intrinsic magnetic properties of $Ce_2Fe_{14}B$ when Fe is replaced by various amounts of Al, Ni, and Si.

2. Materials and Methods

The starting materials were Al (99.7 wt %), B (99.5 wt %), Ce (99.9 wt %), Fe (99.99 wt %), Si (99.9999 wt %), and Ni (99.99 wt %). An argon-arc furnace, equipped with a water-cooled copper crucible and a non-consumable tungsten electrode, was used to prepare the samples. After samples were melted three times to ensure homogeneity, they were sealed in an evacuated quartz tube and annealed at 900 °C for 21 days. These annealing temperature and time were chosen so as to grow high volume percentage of the $Ce_2(Fe_{14-x}T_x)B$ solid solution in each sample. Hitachi S-3400N Scanning Electron Microscopy (SEM) (Hitachi, Tokyo, Japan), combined with wavelength-dispersive X-ray spectroscopy (WDS), was used to analyze compositions, morphologies, and homogeneity ranges of the constituent phases observed in the alloys. X-ray diffraction (XRD) patterns were obtained using a PANanalytical Xpert Pro powder X-ray diffractometer (PANAnalytical, Almelo, The Netherland) with Cu Kα radiation at 45 kV and 40 mA from 20 to 90° 2θ with a 0.02° step size. XRD study of the alloys was carried out using X'Pert HighScore Plus Rietveld analysis software (PANAnalytical, Almelo, The Netherland). Pearson's crystal structure database [33] was used to export the crystallographic data so as to identify the known phases in the samples. Saturation magnetizations (M_S) and anisotropy fields (H_A) were measured using a Quantum Design physical property measurement system (PPMS-9T). The demagnetization data were taken on bulk samples in external fields of up to 50 kOe at 25 °C. H_A was determined by the singular point detection (SPD) method, using second derivative of magnetization (d^2M/dH^2) [34–37]. A Perkin-Elmer 7 Series thermogravimetric analyzer (TGA) was used to determine the Curie temperatures (T_C) of the materials by observing the temperature dependence of the force exerted on the sample in a small magnetic field gradient provided by a permanent magnet placed close to the sample. A nickel metal standard was used to give a transition point reference, and T_C was taken as the point where the magnetization due to the $Ce_2(Fe_{14-x}T_x)B$ vanishes [17,24].

3. Results and Discussion

In this work, the predominant phases observed in the alloys are α-Fe, $Ce_{1.1}Fe_4B_4$, $Ce_2(Fe_{17-x}T_x)$, and $Ce_2(Fe_{14-x}T_x)B$. Annealing at 900 °C increases the growth of $Ce_2(Fe_{14-x}T_x)B$ to above 70%, reducing other phases to insignificant amount as shown in Table 1. $Ce_2(Fe_{14-x}T_x)B$ solid solutions crystallize in the tetragonal $Nd_2Fe_{14}B$-type structure ($P4_2/mnm$, #136 space group). As can be seen in Figure 1, substitution of Fe by Ni and Si, which have smaller atomic radii to Fe, decreases the lattice volumes of the $Ce_2Fe_{14}B$, shifting its peaks positions to higher diffraction angles, whereas Al substitution increases lattice volume of the $Ce_2Fe_{14}B$, shifting its peak positions to lower angles. The measured unit cell parameters and lattice volume of the $Ce_2Fe_{14}B$ used in Figure 1 are in agreement with literature values [4]. The linear relations between lattice parameter c and lattice volume V versus T concentrations in the $Ce_2(Fe_{14-x}T_x)B$ solid solutions are consistent with Vegard's law [38] as shown in Figure 1. The dashed red line in Figure 2 demonstrates the shift in the (140) peak due to substitution of Fe in $Ce_2Fe_{14}B$ by Si, Ni, and Al. This confirms that these elements replace Fe in the $Ce_2Fe_{14}B$ to form solid solutions. Rietveld analysis was carried out on the XRD patterns obtained for all the samples and the relative amount of the $Ce_2(Fe_{14-x}T_x)B$ solid solution is listed in Table 1.
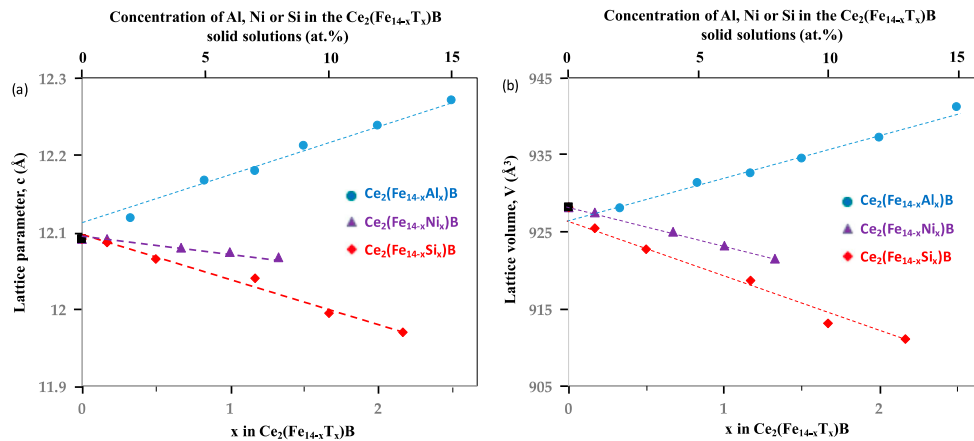
Figure 1. Plots of the (**a**) lattice parameter, c; and (**b**) lattice volume, V, with T content in the $Ce_2(Fe_{14-x}T_x)B$ solid solutions (T = Al, Ni, and Si). The uncertainties in lattice parameter and volume are smaller than the data points.
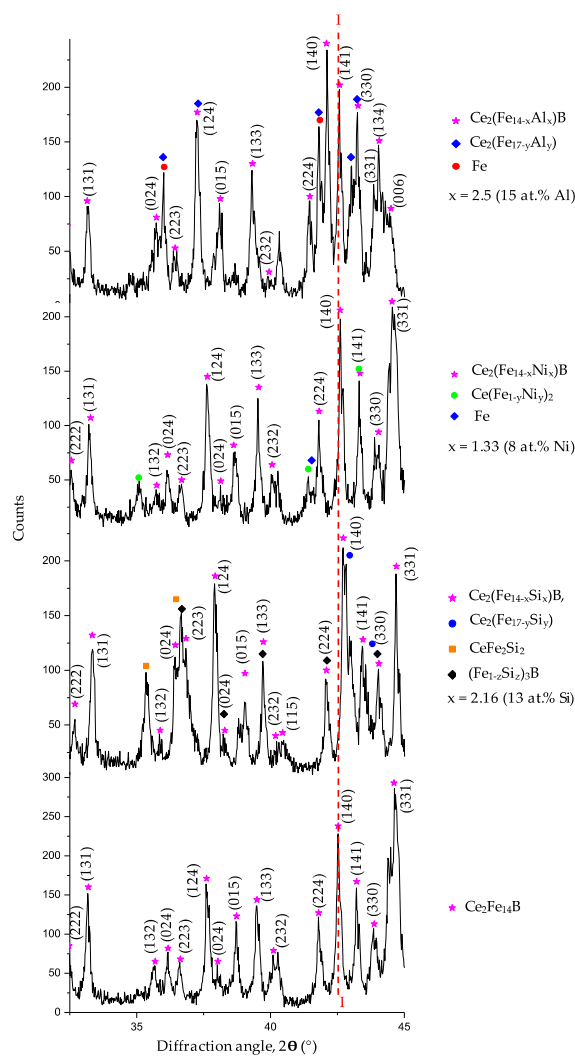

Figure 2. XRD patterns of the $Ce_2Fe_{14}B$ base compound and $Ce_2(Fe_{14-x}T_x)B$ solid solutions. The labelled peaks are for the $Ce_2Fe_{14}B$ and its solid solutions.

In this work, M_S of $Ce_2Fe_{14}B$ at 25 °C was determined as 130 emu/g, and this is approximately 997.1 kA/m using the density of $Ce_2Fe_{14}B$ reported in [4]. This value is somewhat higher than the 931.1 kA/m at 22 °C that was reported for a $Ce_2Fe_{14}B$ single crystal [3,4]. Our value of 28.1 kOe for H_A at 25 °C is also higher than the 26.4 kOe previously reported [5,37] using the same SPD method. This might be due to the presence of other secondary phases, such as iron. This was evident during TGA experiments when the curve did not reach zero force after passing T_C of the $Ce_2Fe_{14}B$ compounds. In addition, the deviation from the single crystal data might be due to the fact that grain size, texture, defects, and precipitates affect many magnetic properties of bulk alloys [39]. The grain boundary increases as the grain size reduces, and increasing or decreasing grain boundaries can either improve or worsen magnetic properties of a material [39–41]. In this work, the annealing conditions were high enough to produce a high volume of $Ce_2(Fe_{14-x}T_x)_{14}B$, and other phases were reduced to minimum amounts. However, grain boundaries were still present in the current samples, and it is expected that the single crystal sample would have had a higher M_S value if the contribution of the secondary phases was ignored. Therefore, the improvement in M_S in this study is presumably attributed to the contributions of the secondary phases. The intrinsic magnetic properties of the $Ce_2(Fe_{14-x}T_x)_{14}B$ solid solutions reported here, where T = Al, Ni, or Si, are limited to the homogeneity ranges, which were determined by diffusion couple and other key alloys techniques described in [32]. Table 1 shows the magnetic properties of these solid solutions in relation to the undoped $Ce_2Fe_{14}B$. The estimated maximum errors in M_S, H_A, and T_C measurements are ±1.4 emu/g, ±2.0 kOe, and ±0.9 °C, respectively.

Table 1. The magnetic properties of $Ce_2(Fe_{14-x}T_x)B$ solid solutions, where T = Al, Ni, or Si.

Key Alloy Number	Dopant Concentration in $Ce_2(Fe_{14-x}T_x)B$ (Atom %)	x	Relative Amount of $Ce_2(Fe_{14-x}T_x)B$ (vol %)	M_S (emu/g) at 25 °C	H_A (kOe) at 25 °C	T_C (°C)
			Ce–Fe–B system			
0	0	0	81.1	130	28.1	151
			Ce–Fe–Al–B system			
1	1.91	0.32	82.1	117.1	27.2	146
2	3.85	0.64	74.6	123.6	22.1	139
3	6.09	1.02	95.0	86.0	16.1	117
4	9.33	1.56	88.0	82.3	10.1	90
5	12.22	2.04	93.7	56.8	3.1	46
6	14.62	2.44	64.0	36.1	-*	72
			Ce–Fe–Ni–B system			
1	1.05	0.18	73.6	127.9	27.1	159
2	2.94	0.49	94.2	124.3	26.1	174
3	6.17	1.03	73.6	114.8	24.1	197
4	8.71	1.45	88.4	106.3	24.1	210
			Ce–Fe–Si–B system			
1	1.30	0.22	91.8	123.1	26.1	163
2	3.75	0.63	84.2	116.1	26.1	183
3	6.62	1.1	83.9	110.4	22.1	200
4	10.04	1.67	86.5	104.2	13.7	219
5	12.62	2.1	96.8	93.0	9.1	243
6	13.60	2.26	78.6	88.8	6.8	252

* The measurement of HA was stopped at Sample #6 because the observed value is already too low for use in a permanent magnet material.

Figure 3 shows the composition dependence of M_S for the $Ce_2(Fe_{14-x}T_x)B$ solid solutions, (T = Al, Ni, or Si). As expected, M_S decreases in all cases as the elements replacing the iron are either non-magnetic (Al and Si) or weakly magnetic (Ni). This behaviour is in agreement with that reported for $RE_2Fe_{14}B$ (RE = rare earth) [27–31,42–47]. The higher apparent M_S value at 3.85 atom % ($x = 0.64$) of Al substituting for Fe in $Ce_2Fe_{14}B$ is due to an α-Fe impurity. This data point was retained as this impurity does not affect the determination of either T_C or H_A. Saturation magnetization shows a

decrease of about 6.2, 2.5, and 2.6 emu/g for Al, Ni, and Si, substituting 1 atom % Fe ($x = 0.17$) in the $Ce_2Fe_{14}B$ compound.
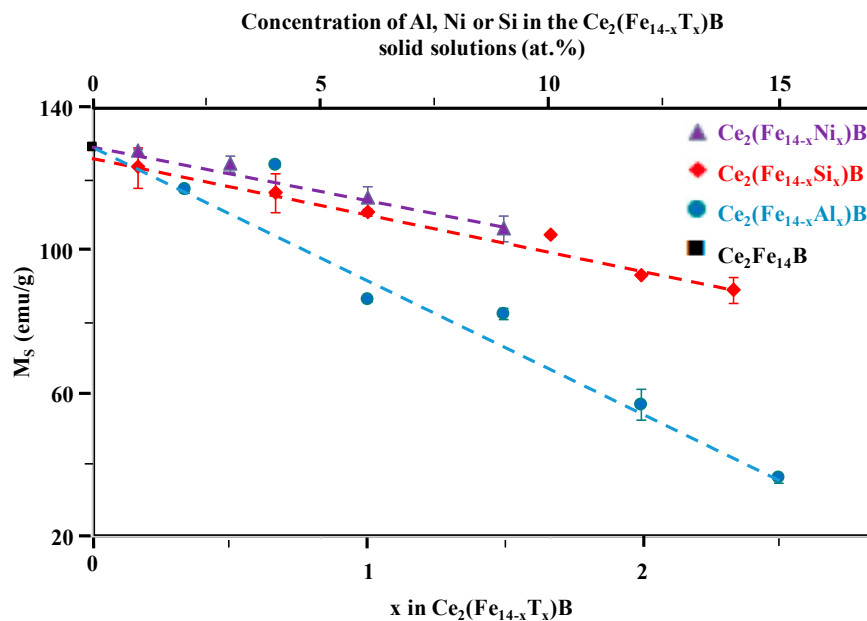

Figure 3. The composition dependence of the saturation magnetization (M_S) for the $Ce_2(Fe_{14-x}T_x)B$ solid solutions ($T = Al$, Ni, Si) at 25 °C. Some error bars are not visible because they are smaller than the data points.

Figure 4 shows the composition dependence of H_A for the $Ce_2(Fe_{14-x}T_x)B$ solid solutions, ($T = Al$, Ni, Si). The anisotropy field generally decreases with increasing Al, Ni, or Si substitution, unlike the work of Jurczyk [43] on the magnetic behaviour of $Nd_2(Fe_{12-x}Al_x)Co_2B$, which showed a maximum H_A of 85 kOe at $x = 0.10$ and 0.30. No such maximum was observed here for $Ce_2(Fe_{14-x}Al_x)B$. Increasing Ni substitution for Fe in $Ce_2Fe_{14}B$ decreased H_A by 0.5(1) kOe for each $x = 0.17$ (1 atom %) substitution of Fe by Ni. Si substitution initially left H_A unchanged at around 26 kOe; however, beyond $x = 0.63$, H_A decreased rapidly. The trend of the plot of H_A for $Ce_2(Fe_{14-x}Si_x)B$ at 25 °C found here differs from that reported for $Nd_2(Fe_{14-x}Si_x)B$ at 22 °C [30], where a maximum was observed at $x = 0.5$ (3 atom % Si). Meanwhile, no maximum was observed here for $Ce_2(Fe_{14-x}Si_x)B$. In general, Ni substitution for Fe in $Ce_2Fe_{14}B$ results in a small overall reduction in H_A, while Al and Si substitutions showed larger reductions.

Figure 5 shows composition dependence of T_C for $Ce_2(Fe_{14-x}T_x)B$, ($T = Al$, Ni, and Si). Replacement of Fe by Al leads to an increase in lattice constant, c, and lattice volume, consequently increasing the distances between Fe sites. This likely leads to a weakening of the Fe–Fe magnetic interactions and T_C falls as the concentration of Al increases. This behaviour is in agreement with previous studies on the effect of Al on other $RE_2Fe_{14}B$ discussed in the literature [29,43]. Ni prefers to substitute for Fe in the $16k_2$ and $8j_2$ sites, and Si prefers $16k_2$ and $8j_2$ sites in $RE_2Fe_{14}B$ [48–50]. Fe substitution by both Ni and Si in $Ce_2Fe_{14}B$ leads to decreases in the lattice constant, c, and the lattice volume. This reduces the distances between the Fe sites, strengthening the magnetic interactions and leading to increases in T_C. At a maximum solubility of 9 atom % Ni ($x = 1.45$), a T_C of 210 °C was measured. We found that Ni substitution leads to an increase of about 7.5 °C per $x = 0.17$ (1 atom % Ni). Increasing Si substitution for Fe in the $Ce_2Fe_{14}B$ compound also increases the T_C almost linearly (about 7.2 °C per $x = 0.17$ (1 atom % Si)) and a T_C of 252 °C was measured in the composition containing the maximum solubility of Si.
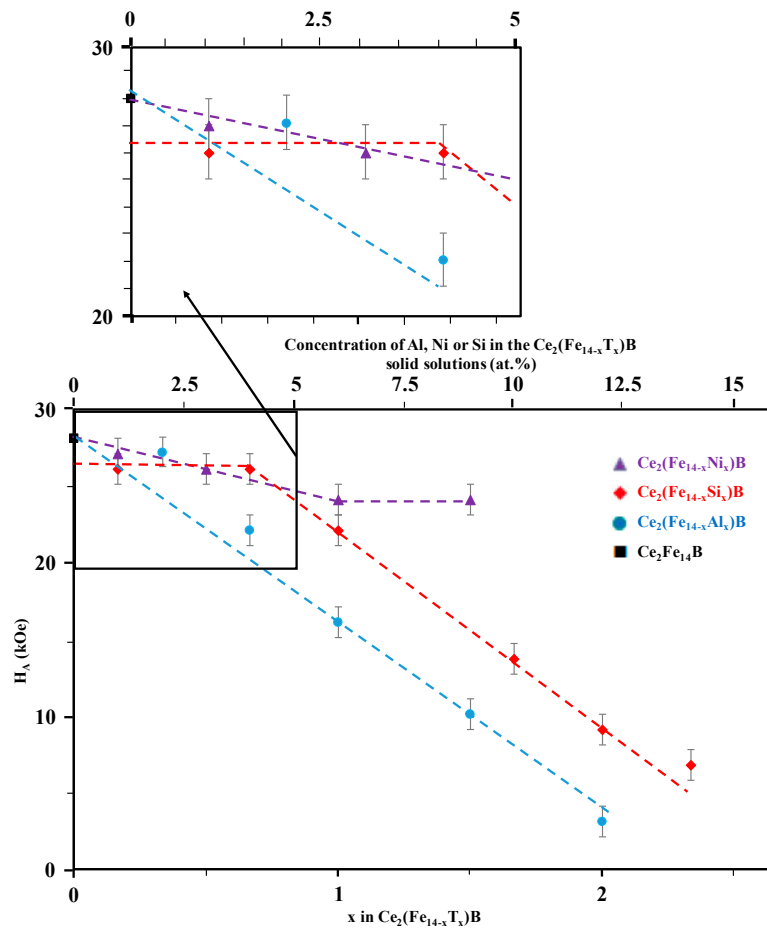
Figure 4. The composition dependence of the anisotropy fields (H_A) for the Ce$_2$(Fe$_{14-x}$T$_x$)B solid solutions (T = Al, Ni, and Si) at 25 °C.
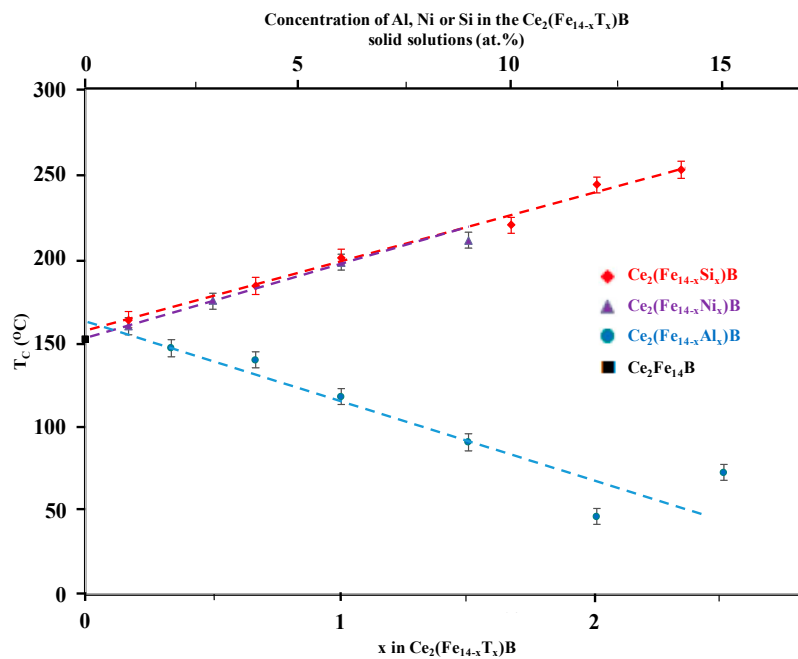

Figure 5. The composition dependence of the Curie temperatures (T_C) for the Ce$_2$(Fe$_{14-x}$T$_x$)B solid solutions (T = Al, Ni, and Si).

4. Conclusions

The influence of Al, Ni, and Si substitutions on the intrinsic magnetic properties of $Ce_2Fe_{14}B$ was studied. We observed that increasing the concentration of Al, Ni, or Si substituting for Fe in $Ce_2Fe_{14}B$ reduces M_S and H_A. Ni or Si substitution increases T_C, while Al reduces it. For $Ce_2Fe_{14}B$ containing Ni, a maximum T_C of 210 °C at $x = 1.45$ (8.71 atom % Ni) was observed, while a higher value of 252 °C was found for $Ce_2Fe_{14}B$ containing $x = 2.26$ (13.60 atom % Si). The lowest value of 46 °C was found for $Ce_2Fe_{14}B$ containing $x = 2.04$ (12.22 atom %) Al. The maximum T_C of 252 °C observed at $x = 2.26$ Si (14 atom %) in the $Ce_2(Fe_{14-x}Si_x)B$ solid solution makes it more promising as a lower cost PM material than the undoped $Ce_2Fe_{14}B$ compound ($T_C = 152$ °C). However, in reality, this might not be the case since the M_S and H_A both decrease with increasing Si content. Therefore, an intermediate composition, with a compromised T_C but with better M_S and H_A might be the most promising Ce–Fe–B magnets containing Ni or Si. Al doping is not recommended because it diminishes all of the studied intrinsic magnetic properties.

Author Contributions: M.M. and F.E.P. conceived the project; M.M. and D.H.R. designed the experiments; K.O. and D.H.R. performed the experiments; K.O., M.M., F.E.P., and D.H.R. analyzed the data; K.O. wrote the paper.

Conflicts of Interest: The authors declare no conflict of interest.

References

1. Hisyam, A.; Ismail, N.A.; Taib, M.K.A.M.; Shariff, S. Leaching study of precious metal recovery from ferric permanent magnet waste. *ARPN J. Eng. Appl. Sci.* **2016**, *11*, 9981–9984.
2. Dupont, D.; Binnemans, K. Recycling of rare earths from NdFeB magnets using a combined leaching/extraction system based on the acidity and thermomorphism of the ionic liquid [Hbet][Tf$_2$N]. *Green Chem.* **2015**, *17*, 2150–2163. [CrossRef]
3. Herbst, J.F.; Meyer, M.S.; Pinkerton, F.E. Magnetic hardening of $Ce_2Fe_{14}B$. *J. Appl. Phys.* **2012**, *111*, 07A718. [CrossRef]
4. Herbst, J. $R_2Fe_{14}B$ materials: Intrinsic properties and technological aspects. *Rev. Mod. Phys.* **1991**, *63*, 819–898. [CrossRef]
5. Grössinger, R.; Sun, X.K.; Eibler, R.; Buschow, K.H.J.; Kirchmayr, H.R. The temperature dependence of the anisotropy field in $R_2Fe_{14}B$ compounds (R = Y, La, Ce, Pr, Nd, Gd, Ho, Lu). *Le J. Phys. Colloq.* **1985**, *46*, C6-221–C6-224. [CrossRef]
6. Herbst, J.F.; Croat, J.J. Neodymium-iron-boron permanent magnets. *J. Magn. Magn. Mater.* **1991**, *100*, 57–78. [CrossRef]
7. Sinnema, S.; Radwanski, R.J.; Franse, J.J.M.; de Mooij, D.B.; Buschow, K.H.J. Magnetic properties of ternary rare-earth compounds of the type $R_2Fe_{14}B$. *J. Magn. Magn. Mater.* **1984**, *44*, 333–341. [CrossRef]
8. Alam, A.; Johnson, D.D. Mixed valency and site-preference chemistry for cerium and its compounds: A predictive density-functional theory study. *Phys. Rev. B* **2014**, *89*, 235126. [CrossRef]
9. Pathak, A.K.; Khan, M.; Gschneidner, K.A., Jr.; Mccallum, R.W.; Zhou, L.; Sun, K.; Dennis, K.W.; Zhou, C.; Pinkerton, F.E.; Kramer, M.J.; et al. Cerium: An unlikely replacement of Dysprosium in high performance Nd–Fe–B permanent magnets. *Adv. Mater.* **2015**, *27*, 2663–2667. [CrossRef] [PubMed]
10. Alam, A.; Khan, M.; Mccallum, R.W.; Johnson, D.D. Site-preference and valency for rare-earth sites in (R-Ce)$_2$Fe$_{14}$B magnets. *Appl. Phys. Lett.* **2013**, *102*, 42402. [CrossRef]
11. Pathak, A.K.; Khan, M.; Gschneidner, K.A., Jr.; Mccallum, R.W.; Zhou, L.; Sun, K.; Kramer, M.J.; Pecharsky, V.K. Magnetic properties of bulk, and rapidly solidified nanostructured $(Nd_{1-x}Ce_x)_2Fe_{14-y}Co_yB$ ribbons. *Acta Mater.* **2016**, *103*, 211–216. [CrossRef]
12. Pathak, A.K.; Gschneidner, K.A., Jr.; Khan, M.; Mccallum, R.W.; Pecharsky, V.K. High performance Nd–Fe–B permanent magnets without critical elements. *J. Alloys Compd.* **2016**, *668*, 80–86. [CrossRef]

13. Li, Z.B.; Shen, B.G.; Zhang, M.; Hu, F.X.; Sun, J.R. Substitution of Ce for Nd in preparing $R_2Fe_{14}B$ nanocrystalline magnets. *J. Alloys Compd.* **2015**, *628*, 325–328. [CrossRef]

14. Yan, C.; Guo, S.; Chen, R.; Lee, D.; Yan, A. Effect of Ce on the magnetic properties and microstructure of sintered Didymium–Fe–B magnets. *IEEE Trans. Magn.* **2014**, *50*, 2102605. [CrossRef]

15. Zhou, C.; Haddad, D.; Kukreja, R.S.; Pinkerton, F.E.; Sun, K.; Kramer, M.J. Magnetic hardening of $CeFe_{11}Ti$ and the effect of TiC addition. *IEEE Trans. Magn.* **2015**, *51*, 2100104. [CrossRef]

16. Zhou, C.; Pinkerton, F.E.; Herbst, J.F. Magnetic properties of $CeFe_{11-x}Co_xTi$ with $ThMn_{12}$ structure. *J. Appl. Phys.* **2014**, *115*, 17C716. [CrossRef]

17. Zhou, C.; Pinkerton, F.E.; Herbst, J.F. High Curie temperature of Ce–Fe–Si compounds with $ThMn_{12}$ structure. *Scr. Mater.* **2015**, *95*, 66–69. [CrossRef]

18. Zhou, C.; Tessema, M.; Meyer, M.S.; Pinkerton, F.E. Synthesis of $CeFe_{10.5}Mo_{1.5}$ with $ThMn_{12}$-type structure by melt spinning. *J. Magn. Magn. Mater.* **2013**, *336*, 26–28. [CrossRef]

19. Zhou, C.; Pinkerton, F.E. Magnetic hardening of $CeFe_{12-x}Mo_x$ and the effect of nitrogenation. *J. Alloys Compd.* **2014**, *583*, 345–350. [CrossRef]

20. Wang, R.; Shen, X.; Liu, Y.; Li, J. Effects of Ga addition on the formability of main phase and microstructure of hot-deformed Ce–Fe–B Magnets. *IEEE Trans. Magn.* **2016**, *52*, 2101806. [CrossRef]

21. Chang-Jiang, Y.; Shuai, G.; Ren-Jie, C.; Dong, L.; A-Ru, Y. Phase constitution and microstructure of Ce–Fe–B strip-casting alloy. *Chin. Phys. B* **2014**, *23*, 107501.

22. Hirosawa, S.; Matsuura, Y.; Yamamoto, H.; Fujimura, S.; Sagawa, M.; Yamauchi, H. Magnetization and magnetic anisotropy of $R_2Fe_{14}B$ measured on single crystals. *J. Appl. Phys.* **1986**, *59*, 873–879. [CrossRef]

23. Wang, X.; Zhu, M.; Li, W.; Zheng, L.; Zhao, D.; Du, X.; Du, A. The microstructure and magnetic properties of melt-spun CeFeB ribbons with varying Ce content. *Electron. Mater. Lett.* **2015**, *11*, 109–112. [CrossRef]

24. Skoug, E.J.; Meyer, M.S.; Pinkerton, F.E.; Tessema, M.M.; Haddad, D.; Herbst, J.F. Crystal structure and magnetic properties of $Ce_2Fe_{14-x}Co_xB$ alloys. *J. Alloys Compd.* **2013**, *574*, 552–555. [CrossRef]

25. Xing, M.; Han, J.; Lin, Z.; Wan, F.; Li, C.; Liu, S.; Wang, C.; Yang, J.; Yang, Y. Anisotropic ternary $Ce_{13}Fe_{80}B_7$ powders prepared by hydrogenation–disproportionation–desorption–recombination process and the diffusion of Ce–Cu eutectic alloys. *J. Magn. Magn. Mater.* **2013**, *331*, 140–143. [CrossRef]

26. Zhang, M.; Shen, B.; Hu, F.; Sun, J. The effect of Si substitution on structure and magnetic properties in Mischmetal–Fe–B ribbons. In Proceedings of the 2015 IEEE International Magnetics Conference (INTERMAG), Beijing, China, 11–15 May 2015.

27. Hirosawa, S.; Yamaguchi, Y.; Tokuhara, K.; Yamamoto, H.; Fujimura, S.; Sagawa, M. Magnetic properties of $Nd_2(Fe_{1-x}M_x)_{14}B$ measured on single crystals (M = Al, Cr, Mn and Co). *IEEE Trans. Magn.* **1987**, *23*, 2120–2122. [CrossRef]

28. Kowalczyk, A.; Stefanski, P.; Wrzeciono, A.; Szlaferek, A. Structure and magnetic properties of $R_2Fe_{14-x}Ni_xB$ compounds (R = Nd and Gd). *Phys. Status Solidi* **1989**, *114*, 355–358. [CrossRef]

29. Kou, X.C.; Sun, X.K.; Chuang, Y.C.; Zhao, T.S.; Grossinger, R.; Kirchmayr, H.R. Exchange interaction and magnetic anisotropy in $Nd_2(Fe_{13}M)B$ compounds (M = Ga, Si, Al). *J. Magn. Magn. Mater.* **1989**, *82*, 327–334. [CrossRef]

30. Jurczyk, M.; Kowalczyk, A.; Wrzeciono, A. Magnetic properties of $Nd_2Fe_{14-x}Si_xB$ compounds. *Phys. Status Solidi* **1987**, *101*, K65. [CrossRef]

31. Jurczyk, M.; Kowalczyk, A. Effect of silicon additions on the magnetic properties of $Nd_2Fe_{12}Co_2B$ alloy. *J. Magn. Magn. Mater.* **1987**, *68*, 331–334. [CrossRef]

32. Orimoloye, K.; Kevorkov, D.; Medraj, M. Phase equilibria and magnetic phases in the Fe-rich regions of the Fe-Ce-{Ni, Si, Al}-B quaternary systems. *J. Alloys Compd.* **2017**. submitted.

33. Putz, H.; Brandenburg, K. *Pearson's Crystal Data. Crystal Structure Database for Inorganic Compounds*; CD-ROM Software Version 1.3; ASM International: Materials Park, OH, USA, 2007.

34. Asti, G.; Rinaldi, S. Nonaliticity of the magnetization curve: Application to the measurement of anisotropy in polycrystalline samples. *Phys. Rev. Lett.* **1972**, *28*, 1584–1586. [CrossRef]

35. Asti, G.; Rinaldi, S. Singular points in the magnetization curve of a polycrystalline ferromagnet. *J. Appl. Phys.* **1974**, *45*, 3600–3610. [CrossRef]

36. Liu, X.; Ryan, D.H.; Wang, M.; Lu, Q.; Zhang, H. Experimental and first-principles determination of the magnetocrystalline anisotropy in MnxGa. *AIP Adv.* **2017**, *7*, 56216. [CrossRef]

37. Grossinger, R.; Sun, X.K.; Eibler, R.; Buschow, K.H.J.; Kirchmayr, H.R. Temperature dependence of anisotropy fields and initial susceptibilities in $R_2Fe_{14}B$ compounds. *J. Magn. Magn. Mater.* **1986**, *58*, 55–60. [CrossRef]

38. Denton, A.R.; Ashcroft, N.W. Vegard's law. *Phys. Rev. A* **1991**, *43*, 3161–3164. [CrossRef] [PubMed]

39. Yu, R.H.; Basu, S.; Zhang, Y.; Parvizi-Majidi, A.; Xiao, J.Q. Pinning effect of the grain boundaries on magnetic domain wall in FeCo-based magnetic alloys. *J. Appl. Phys.* **1999**, *85*, 6655–6659. [CrossRef]

40. Landgraf, J.F.G.; Filipini da Silvera, J.R.; Rodrigues, D., Jr. Determining the effect of grain size and maximum induction upon coercive field of electrical steels. *J. Magn. Magn. Mater.* **2011**, *323*, 2335–2339. [CrossRef]

41. Tong, H.Y.; Shi, F.G. Magnetic properties of polycrystalline FeBSi alloys with ultrafine grains. *Scr. Mater.* **1996**, *34*, 1887–1892. [CrossRef]

42. Burzo, E.; Plugaru, N.; Pop, V.; Stanciu, L.; Wallace, W.E. Bulk magnetic properties of the $Y_2T_xFe_{14-x}B$ compounds, where T = Al, Ni, or Co. *Solid State Commun.* **1986**, *58*, 803–805. [CrossRef]

43. Jurczyk, M. On the magnetic behaviour of $Nd_2Fe_{12-x}T_xCo_2B$ compounds (T = Al, V, Cr). *IEEE Trans. Magn.* **1988**, *24*, 1942–1944. [CrossRef]

44. Bolzoni, F.; Leccabue, F.; Moze, O.; Pareti, L.; Solzi, M. Magnetocrystalline anisotropy of Ni and Mn substituted $Nd_2Fe_{14}B$ compounds. *J. Magn. Magn. Mater.* **1987**, *67*, 373–377. [CrossRef]

45. Ku, H.C.; Yen, L.S. Magnetic properties of the new permanent magnet compounds $Nd_2(Fe_{0.9}M_{0.1})_{14}B$ (M = Sc, Ti, V, Cr, Mn, Co, Ni). *J. Less Common Met.* **1987**, *127*, 43–48. [CrossRef]

46. Burzo, E.; Stanciu, L.; Wallace, W.E. On the magnetic behaviour of $Y_2Fe_{14-x}Ni_xB$ and $Y_2Fe_{14-x}Co_xB$. *J. Less Common Met.* **1985**, *111*, 83–86. [CrossRef]

47. Pedziwiatr, A.T.; Wallace, W.E.; Burzo, E.; Pop, V. Magnetic properties of $Y_2Fe_{14-x}M_xB$ compounds where M = Si or Cu. *Solid State Commun.* **1987**, *61*, 61–64. [CrossRef]

48. Dai, S.; Morrish, A.H.; Zhou, X.Z.; Hu, B.P.; Zhang, S.G. Mossbauer study of the permanent magnet material $Nd_2(Fe_{1-x}Ni_x)_{14}B$. *J. Appl. Phys.* **1988**, *63*, 3722–3724. [CrossRef]

49. Marasinghe, G.K.; Pringle, O.A.; Long, G.J.; Yelon, W.B.; Grandjean, F. A neutron diffraction and Mössbauer spectral study of the structure and magnetic properties of the $Y_2Fe_{14-x}Si_xB$ solid solutions. *J. Appl. Phys.* **1994**, *76*, 2960–2968. [CrossRef]

50. Marasinghe, G.K.; Pringle, O.A.; Long, G.J.; James, W.J.; Xie, D.; Li, J.; Yelon, W.B.; Grandjean, F. Neutron diffraction and Mössbauer effect study of the preferential silicon site occupation and magnetic structure of $Nd_2Fe_{14-x}Si_xB$. *J. Appl. Phys.* **1993**, *74*, 6798–6809. [CrossRef]